INL/EXT-17-43110

Light Water Reactor Sustainability Program

Modeling of Cu Precipitate Contributions to Reactor Pressure Vessel Steel Microstructure Evolution and Embrittlement

Stephanie A. Pitts
Xianming Bai
Yongfeng Zhang

August 2017

DOE Office of Nuclear Energy

INL/EXT-17-43110

Light Water Reactor Sustainability Program

Modeling of Cu Precipitate Contributions to Reactor Pressure Vessel Steel Microstructure Evolution and Embrittlement

Stephanie A. Pitts[1]
Xianming Bai[2]
Yongfeng Zhang[1]

[1]Idaho National Laboratory, [2]Virginia Tech

August 2017

Idaho National Laboratory
Idaho Falls, Idaho 83415

http://www.inl.gov/lwrs

Prepared for the
U.S. Department of Energy
Office of Nuclear Energy
Under DOE Idaho Operations Office
Contract DE-AC07-05ID14517

ABSTRACT

This report summarizes efforts during FY 2017 for developing capabilities to simulate microstructure evolution and the resulting embrittlement in reactor pressure vessel steels. During operation, reactor pressure vessels undergo hardening and embrittlement due to irradiation induced defect accumulation and irradiation enhanced solute precipitation, including copper rich precipitate formation. Both defect production and solute precipitation begin on the atomic scale, and the effects of these irradiation defects later manifest as as degradation in the engineering scale properties. Modeling and simulation capabilities are being developed at multiple scales to better understand these mechanisms and their effects on engineering-scale material response. Much of the work performed during this year and presented here is to couple these microstructure evolution models with each other; these coupling efforts have focused on copper rich precipitate formation and impact on macroscale embrittlement. These efforts include the development of a coupled capability with lattice kinetic Monte Carlo and rate theory models to capture irradiation enhanced diffusion in the formation of defects. In addition, a cluster dynamics model to predict Cu precipitate formation was implemented in Grizzly. Finally, crystal plasticity models in Grizzly to predict the effect of Cu precipitates on reactor pressure steel hardening were improved and coupled with cluster dynamics models.

CONTENTS

1 Introduction **1**

2 Irradiation enhanced Cu precipitation in RPV steel alloys **2**
2.1 Model description 2
2.2 Results 3
2.3 Discussion and conclusions 3

3 Implementation of Cluster Dynamics Model of Cu Precipitation in Grizzly **5**
3.1 Cluster dynamics model description 5
3.2 Model implementation in Grizzly 7
3.3 Code verification using two case studies 9
3.4 Discussions and conclusions 12

4 Cu precipitate induced embrittlement in crystal plasticity **13**
4.1 Model description and implementation 13
4.2 Cross slip formulation comparison 14
4.3 Coupling to cluster dynamics CRP results 16
4.4 Discussion and conclusions 17

5 Summary **18**

6 References **19**

FIGURES

1 Evolution of vacancy and CRP concentrations under thermal aging and irradiation conditions. 3
2 Time evolution of interstitial and vacancy concentration under electron and neutron irradiation. 11
3 Evolution of Cu precipitation formation kinetics in Fe-1.34at.%Cu under electron irradiation. 11
4 Evolution of Cu precipitation formation kinetics in Fe-1.34at.%Cu under neutron irradiation. 12
5 Comparison of deterministic and stochastic dislocation cross slip models under multiple slip system activation loading conditions. 15
6 Comparison of deterministic and stochastic dislocation cross slip models under single slip system activation loading conditions. 16
7 Response of coupled crystal plasticity and cluster dynamics simulation to various neutron irradiation doses. 17

TABLES

1 Cluster dyanmics model parameters for Cu precipitation in F3-1.34at.%Cu under electron and neutron irradiation. 10
2 Crystal plasticity model parameters calibrated for Fe-0.3%Cu with experimental data [16] . . 15

ACRONYMS

AKMC	atomic kinetic Monte Carlo
APT	atom probe tomography
BCC	body centered cubic
BWR	boiling water reactor
CD	cluster dynamics
CDF	continuous distribution function
CPFEM	crystal plasticity finite element method
CRP	copper rich precipitate
DD	dislocation dynamics
DFT	density functional theory
dpa	displacement per atom
FE	finite element
FP3DM	Frenkel pair three-dimensional diffusion model
LKMC	lattice kinetic Monte Carlo
MD	molecular dynamics
MNP	Mn/Ni rich precipitate
ODE	ordinary differential equation
PAS	positron annihilation spectroscopy
PDE	partial differential equation
PF	phase field
PWR	pressurized water reactor
RPV	reactor pressure vessel
RT	rate theory
SIA	Self Interstitial Atoms
SPPARKS	Stochastic Parallel PARticle Kinetic Simulator
TEM	transmission electron microscopy

1 Introduction

Maintaining the integrity of reactor pressure vessels (RPVs) is a key requirement for the safe long term operation of existing reactor fleets: RPVs house the reactor core and are expensive to be replaced. That the RPV steel remains sufficiently tough and ductile to resist crack growth under operating temperature and irradiation conditions is an important safety criterion [1]. RPVs are typically made of iron-based steels, with copper as either an alloying element or an impurity. These alloying elements tend to form solute precipitate clusters, in the case of copper termed CRPs (copper rich precipitates), and these CRPs are considered to be one of the key contributors to irradiation-induced embrittlement [2, 3]. Irradiation embrittlement is characterized by an increase in the ductile-to-brittle transition temperature (DBTT) [1], indicating a higher tendency for brittle fracture behavior to occur at higher temperatures. The CRP formation is accelerated by interstitial and vacancy concentrations, leading to high densities of irradiation-induced precipitates. The vacancies (unoccupied lattice sites) and interstitials (extra atoms on lattice sites) are lattice point defects generated by high energy neutrons during normal operation. All of these irradiation defects impede dislocation motion, reducing ductility and increasing the hardening and embrittlement of RPVs [4]. Increased embrittlement can increase the propensity of RPVs to fail.

To reliably assess the safe long term operation of existing reactors, quantitative and physics-based correlations between irradiation dose levels and embrittlement are needed for given reactor operating conditions. Because engineering scale material properties are determined by the microstructure, the development of these correlations requires simulation tools to describe the evolution of the RPV microstructure under continuing irradiation exposure. These microstructural features evolve with time and depend on the irradiation and thermal histories. For RPV steels the critical microstructure evolution features are those representing radiation damage and solute precipitates, including their volumetric density, size distribution, and spatial distribution. The evolution of radiation damage, vacancy and interstitial generation, and CRP formation are physically coupled with each other. Because the formation of CRPs is accelerated by the transient irradiation-induced vacancy concentration and because the specific characteristics of the CRPs determine the degree to which these precipitates contribute to the macroscale embrittlement of RPV steel, a multi-scale simulation approach is required to understand the effect of CRPs on RPV embrittlement. In previous years, simulation models for different length and time scale aspects of the CRP microstructure formation have been developed [5, 6, 7], and coupling among these individual simulations models is now necessary to better understand the role of copper rich precipitate formation on the microstructure evolution and resulting plastic embrittlement.

To model the formation and growth of lattice point defects, e.g. vacancies, and the CRPs, rate theory (RT) and cluster dynamics (CD) approaches are implemented while continuum mesoscale crystal plasticity models are used to model the impact of these defects on RPV toughness. The acceleration of CRP formation by irradiation-induced diffusion is modeled by coupling lattice kinetic Monte Carlo (LKMC) and rate theory (RT) models. The effect of specific CRP characteristics created by different irradiation doses on macroscale hardening and embrittlement is captured by coupling crystal plasticity with the results of cluster dynamics simulations. The development of these models spans several years, and more detail on this ongoing effort can be found in the previous Grizzly reports [5, 8, 9, 6, 7]. In this document, the effort made in FY17 to couple individual microstructure models is summarized.

2 Irradiation enhanced Cu precipitation in RPV steel alloys

Two main drivers of microstructure evolution of RPV steels are the accumulation of radiation damage and the precipitation of solute elements [10]. Under irradiation, these two effects are strongly coupled with each other. In particular, the precipitation kinetics of alloying elements can be dramatically accelerated by irradiation produced defects such as vacancies. This acceleration occurs because most alloying elements are substitution elements in BCC steels, and these substitution alloy elements diffuse by a vacancy-mediated mechanism. The effective diffusivities of alloying elements are proportional to the transient vacancy concentration, and, in irradiation conditions, the transient vacancy concentration is much higher than the thermal equilibrium concentration. Therefore, precipitation can occur with a much higher rate under irradiation compared to the rate from thermal aging. This rate acceleration effect has to be considered to predict the precipitation kinetics in RPV steels under neutron irradiation.

2.1 Model description

In previous years, an lattice kinetic Monte Carlo (LKMC) model has been developed for alloying element precipitation in body centered cubic (BCC) crystal steels. This method has been used to simulate the formation of Cu-rich precipitates (CRPs) in model alloys during thermal aging, and the possible formation of Mn-Ni-rich precipitates (MNPs) at irradiation-induced defects [8, 6, 7]. The results of the CRP formation model have been benchmarked with thermal aging experiments in FeCu1.34% model alloy. One critical component that is missing in applying this model under neutron irradiation conditions is the irradiation enhanced diffusion. The ability to include irradiation enhanced diffusion requires the transient vacancy concentration: the individual vacancies responsible for alloying element diffusion under an irradiating environment. This transient concentration information can be obtained by coupling the LKMC model with the rate theory (cluster dynamics) model, and the cluster dynamics model is being developed in parallel for radiation damage accumulation under the Grizzly project. In FY17, an effort was made to couple the LKMC and rate theory models.

In LKMC simulations a constant vacancy concentration (c_v) is used, which differs from both the thermal equilibrium concentration and the transient concentration under irradiation, because of the limitations in time and spatial scales of the simulation. To accommodate the use of variable vacancy concentrations, the LKMC time needs to be converted to physical time. This conversion requires the thermal equilibrium c_v for thermal aging, and the transient c_v for irradiation. The relation between LKMC time and physical time is given by:

$$dt_{real} = dt_{KMC} \frac{fvt * c_v^{KMC}}{c_v^{real}} \tag{1}$$

Here t_{real} is the physical time in realistic materials, and t_{KMC} that in KMC simulations. Accordingly c_v^{real} and c_v^{KMC} are the realistic vacancy concentration and that in a KMC simulation. The conversion is straightforward for thermal aging since the c_v^{real} is constant at a given temperature, and the coefficient fvt accounts for the effect of impurity trapping [6]. Under irradiation, the vacancy concentration changes with time without an analytical solution. Therefore, direct conversion is not feasible. Instead, the KMC time can be correlated to the physical time by:

$$\int_0^{t_{KMC}} fvt * c_v^{KMC} dt_{KMC} = \int_0^{t_{real}} c_v^{real} dt_{real} \tag{2}$$

The integrated $c_v * dt$ denotes the effective vacancy diffusion in a given time period. Provided that the transient c_v^{real} is known, numerical solution can be obtained to convert the KMC time to physical time under irradiation.

2.2 Results

To demonstrate this coupling, we used the vacancy concentration given by the rate theory (see Section 3) [11]. The irradiation condition is at 500^{o}C with a dpa rate of 2.0×10^{-9}dpa/s. We note that the existence of Cu will change the diffusion of vacancy compared to the rate in pure BCC Fe. The effect has been considered in the rate theory. More details about the rate theory (or cluster dynamics) model are given in Section 3. As shown in Figure 1, to reach the same effective vacancy diffusion, a significantly longer time is needed under thermal aging than under irradiation due to the much lower vacancy concentration. To further demonstrate the irradiation enhanced CRP precipitation, the previous LKMC results in a FeCu1.34% model alloy are re-plotted by converting the KMC time to the physical time under both thermal aging and irradiation. The irradiation is at 500^{o}C with a dpa rate of 2.0×10^{-9}dpa/s. For thermal aging the thermal equilibrium vacancy concentration is calculated using a vacancy formation energy of 1.60 eV. For irradiation, the transient vacancy concentration is obtained from the rate theory. As shown in Figure 1, to reach the peak in CRP concentration requires approximately 50 seconds under irradiation, while it takes nearly 1 hour under thermal aging at the same temperature to reach the peak concentration value. This result indicates the importance of including irradiation enhanced diffusion in predicting the precipitation kinetics of alloying elements in RPV steels.

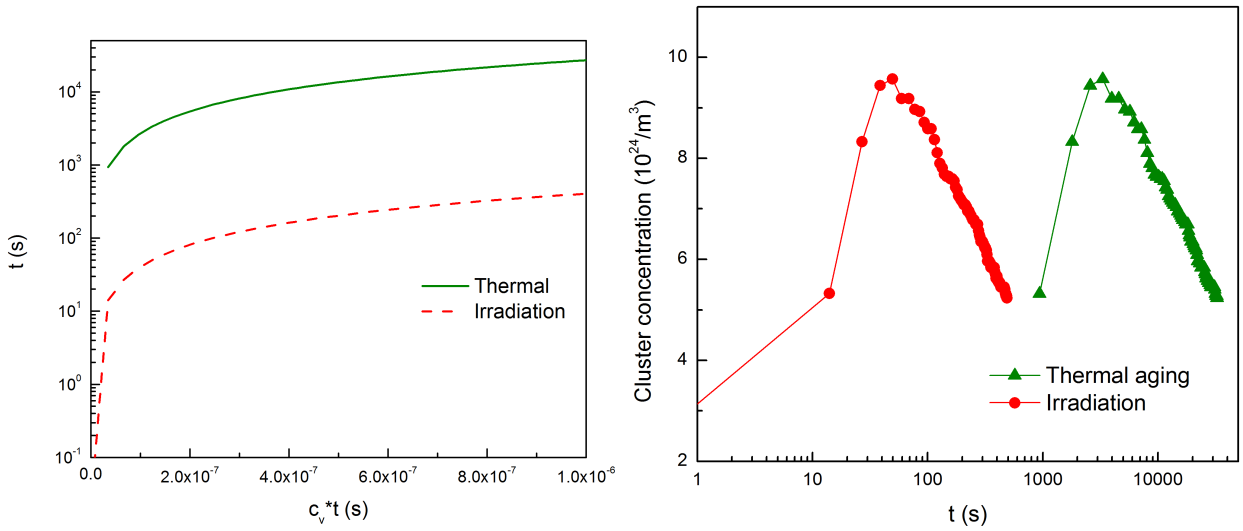

Figure 1: (left) Comparison of the time required to reach the same integrated $c_v * t$ value during thermal aging and irradiation, and (right) volumetric density of CRPs with 50 or more Cu atoms as a function of time under irradiation. The CRPs precipitation is simulated using LKMC with a simulation cell of 28.5 by 28.5 by 28.5 nm^3. It contains 2M atoms with one vacancy. The KMC time is then converted to physical time using the vacancy concentration from the rate theory.

2.3 Discussion and conclusions

The above results demonstrate the importance of irradiation-enhanced precipitation and the capability of coupling LKMC and rate theory (or cluster dynamics) to account for the enhanced precipitation due to irradiation. This coupling represents a critical component for predicting the precipitation kinetics of alloying elements in an irradiating environment. Some discussion is warranted here. First, in Figure 1 the rate theory model rather than the more complicated cluster dynamics model is used to estimate the transient vacancy concentration. In the former model all vacancies are regarded as individual without forming clusters, while in the latter clusters of various sizes are considered. In general, large vacancy clusters have lower diffusivities

than individual ones. Therefore, using the rate theory model may over estimate the effective diffusivity. Because of its much higher solving speed, the rate theory model serves well for the purpose of demonstrating the coupling with LKMC. More realistic assessments can be obtained by using the solutions from cluster dynamics. Second, the effect of irradiation-induced segregation/precipitation of alloying elements are ignored here. This effect can be considered by accounting for the transient information of defect clusters into LKMC, with the interaction between these defects and alloying elements calculated by density functional theory calculations or molecular dynamics simulations [12]. This capability will be demonstrated in the future.

3 Implementation of Cluster Dynamics Model of Cu Precipitation in Grizzly

Reactor pressure vessels (RPV) are exposed to long-term neutron irradiation during their service [10]. Neutron irradiation can induce the precipitation of alloy elements such as Cu in RPV steels. These precipitates are typically a few nanometers in diameter. Despite their small size, they can act as strong obstacles for dislocation motion, leading to radiation hardening and embrittlement [2]. Currently it is well accepted that Cu precipitates are the main contributor to the degradation of the mechanical integrity in RPVs. Therefore, integration of a Cu precipitation model in Grizzly can provide a more science-based prediction of the radiation-induced degradation of mechanical properties in RPV compared to the traditional empirical approaches. In FY2016, the Grizzly team had developed a calibrated cluster dynamics model of Cu precipitation under irradiation and the model had been tested in a standalone code [7]. In FY17, the model has been integrated into the MOOSE based Grizzly code as described below.

3.1 Cluster dynamics model description

The cluster dynamics method can model the nucleation, growth, and coarsening of solute precipitation in the same framework, and radiation effects can also be conveniently included in the model [13]. The model implemented in our work is mainly based on a previously published work in literature [13]. The details of the model are also described in a recently accepted manuscript [11]. Here the key information of the model is presented so that the implementation methodology can be explained clearly in a self-contained manner. This description may also help future Grizzly users better understand the physical meaning of the input parameters.

During precipitation, Cu clusters can have different sizes. In cluster dynamics modeling, the size of each class of cluster can be represented by the number of atoms it contains. Each class of cluster has a concentration based on the mean field assumption. The concentration of a cluster containing n Cu atoms is represented by C_n. Here only Cu monomers are considered mobile. When a cluster of size n absorbs one Cu monomer, its size becomes $n+1$. When a cluster of size $n+1$ emits one Cu monomer through thermal emission, its size decreases to n. Therefore, the flux from cluster size n to $n+1$ is:

$$J_{n\rightarrow n+1} = \beta_n C_1 C_n - \alpha_{n+1} C_{n+1}, \tag{3}$$

where β_n is the absorption coefficient for a cluster of size n and α_{n+1} is the emission coefficient for a cluster of size $n+1$. Assuming all clusters (including monomers) have a spherical geometry, the radius of a cluster of size n is $r_n = \left[\frac{3nV_{at}}{4\pi}\right]^{1/3}$, where $V_{at} = {a_0}^3/2$ is the volume per BCC Cu (or Fe because of the assumption of coherent interface) atom and a_0 is the lattice parameter for BCC Fe. The absorption coefficient β_n has the form

$$\beta_n = \frac{4\pi(r_1 + r_n)D_{Cu}}{V_{at}}, \tag{4}$$

where D_{Cu} is the Cu diffusion coefficient in Fe matrix. The emission coefficient is exponentially related to the absorption coefficient by the binding energy of the Cu cluster (E^b), the Boltzmann constant (k_B), and the temperature (T):

$$\alpha_{n+1} = \beta_n \exp\left[-\frac{E^b_{n+1}}{k_B T}\right]. \tag{5}$$

In Equation 5, the cluster binding energy E^b is size-dependent and related to the cluster interface energy σ. The binding energy for a cluster size of $n+1$ is

$$E^b_{n+1} = \Omega - T\Delta S - (36\pi)^{1/3} V_{at}^{2/3} \sigma[(n+1)^{2/3} - n^{2/3}], \tag{6}$$

where Ω is the mixing enthalpy and ΔS is non-configurational entropy [13], respectively. The binding energy increases with cluster size and gradually approaches a saturated value. The concentration of each cluster size (C_n) evolves dynamically with time through either absorbing or emitting a Cu monomer. The time evolution of C_n is described by a rate theory equation,

$$\frac{dC_n}{dt} = J_{n-1\to n} - J_{n\to n+1}, (n \geq 2). \tag{7}$$

For the evolution of the concentration of the monomer (C_1), the situation is more complex because it is related to all $n \geq 2$ fluxes. In addition, the formation or dissociation of a di-Cu cluster involves two Cu monomers at each time. Considering the role of C_1 in these processes, the time evolution of C_1 can be represented as:

$$\frac{dC_1}{dt} = -2J_{1\to 2} - \sum_{n\geqslant 2}^{\infty} J_{n\to n+1}. \tag{8}$$

Equations 7 and 8 describe the time evolution of all cluster sizes (n = 1 - ∞). Practically, a maximum cluster size n_{max} is used and its flux is set to zero as the boundary condition. Solving these ordinary differential equations (ODEs), the concentration of each cluster size (C_n) can be obtained as a function of time. Since Cu atoms form substitution alloys in Fe, the Cu diffusion in Fe is mediated by vacancies. Under irradiation, vacancy concentration can be much higher than the thermal vacancy concentration. As a result, Cu diffusion is enhanced by irradiation. The radiation-enhanced Cu diffusivity is

$$D^{irr}_{Cu} = D^{th}_{Cu} \cdot \frac{C^{irr}_v}{C^{th}_v} = D^{th}_{Cu} \cdot f_{irr}, \tag{9}$$

where the superscripts th and irr represent the thermal and irradiation conditions, respectively, for vacancy concentration (C_v) and Cu diffusion coefficient (D_{Cu}). The ratio of $C^{irr}_v / C^{th}_v = f_{irr}$ is the radiation-enhanced factor for Cu diffusion. The temperature-dependent thermal diffusion coefficient of Cu can be described by $D^{th}_{Cu} = D^0_{Cu} \exp\left(-\frac{E^m_{Cu}}{k_B T}\right)$, where D^0_{Cu} and E^m_{Cu} are the prefactor and activation energy of Cu diffusion in BCC Fe, respectively. The thermal vacancy concentration is related to the vacancy formation energy (E^f_v) in Fe and to the temperature by $C^{th}_v = \exp\left(-\frac{E^f_v}{k_B T}\right)$. The vacancy concentration under irradiation (C^{irr}_v) depends on defect production rate, defect reaction, and defect loss to sinks. As in Ref. [13], here a simplified rate theory model is used to describe the point defect evolution under irradiation. In this model, only defect production, defect recombination, and defect loss to dislocations are considered. The time evolution of interstitial concentration (C_i) and vacancy concentration (C_v) are described by the following two rate equations,

$$\frac{dC_i}{dt} = \epsilon G_0 - k_{iv} C_i C_v - z_i D_i C_i \rho_d, \tag{10}$$

$$\frac{dC_v}{dt} = \epsilon G_0 - k_{iv} C_i C_v - z_v D_v C_v \rho_d, \tag{11}$$

where ϵ is cascade efficiency; G_0 is defect production rate or irradiation dose rate; k_{iv} is defect recombination coefficient between interstitials and vacancies; $D_v = D^0_v \exp\left(-\frac{E^m_v}{k_B T}\right)$ is temperature-dependent Fe vacancy

diffusion coefficient, where D_v^0 and E_v^m are the prefactor and migration energy for vacancy diffusion, respectively; A similar equation of $D_i = D_i^0 \exp\left(-\frac{E_i^m}{k_B T}\right)$ is used for Fe interstitial diffusion coefficient; ρ_d is dislocation density; and z_i and z_v are the absorption efficiencies for interstitials and vacancies, respectively. Typically it is assumed $z_i > z_v$. By solving Equations 10 and 11, the time evolution of vacancies and interstitials under irradiation can be obtained. This then permits the calculation of radiation-enhanced Cu diffusion using Equation 9.

3.2 Model implementation in Grizzly

The implemented cluster dynamics model in Grizzly takes advantage of some MOOSE features such as *UserObject*, *Actions*, *Postprocessor*, *ScalarKernel*. A test problem directory was created to verify the implemented codes. The test input file in this directory can be easily modified to study Cu precipitation under different conditions. The names of all classes start with 'CDCu' to indicate cluster dynamics of Cu precipitation. The classes implemented in Grizzly are described below.

CDCuParameters class. This class is derived from the *GeneralUserObject* class. As its name implies, it stores many constant parameters for the model. Most of the input parameters of the cluster dynamics model are read by this class, such as T, a_0, etc. The class uses the input parameters to further calculate some other parameters such as the size-dependent absorption coefficient β_n (Equation 4), the emission coefficient α_n (Equation 5), the binding energy E_n^b (Equation 6), the diffusion coefficients of a Cu atom, etc. These properties are stored in this *UserObject* class so that it is convenient for other classes to access them.

CDCuBase class. This class is derived from the *ODEKernel* class. It is the base kernel class for solving the ordinary differential equations of the Cu cluster evolution (Equations (7) and (8)). This class accesses the *CDCuParameters* class to get the necessary parameters for solving the cluster evolution equations. Note that this base class accesses the absorption coefficient β_n array and the emission coefficient α_n array using constant references. Therefore all the cluster evolution kernels derived from this base class access the same memory of the two arrays in the *UserObject*. This approach is important when the maximum cluster size is large because each cluster dose not need allocate its own memory for these two arrays.

CDCuC1 class. This class is derived from the *CDCuBase* class. It is the *ODE kernel* for the Cu monomer (C_1), which solves Equation 8. C_1 couples with all other C_n clusters for $n \geq 2$. Both Jacobian and OffDiagonalJacobian functions are implemented for this class, which enable accurate preconditioning and good convergence.

CDCuCn class. This class is also derived from the *CDCuBase* class. It is the *ODE kernel* for all $n \geq 2$ Cu clusters (C_n), which solves Equation 7. Each C_n only couples with its previous cluster C_{n-1} and its following cluster C_{n+1}. Both *Jacobian* and *OffDiagonalJacobian* functions are implemented for this class.

CDCuPrecipitation class. This class is derived from the *Action* class. It creates all the Variables ($C_1 - C_n$), ScalarKernels (*CDCuC1* and *CDCuCn*), *ODETimeDerivative* Kernels, and sets the initial conditions for all variables. It also creates a *UserObject* of the *CDCuParameters* type called *UO_Parameters*. Therefore, the setup of the cluster dynamics model is mostly conducted in this action. It greatly simplifies the syntax of the input file and makes the code user-friendly.

CDCuClusterAverage class. This class is derived from the *GeneralPostprocessor* class. It post-processes the simulation data and outputs the time-dependent Cu monomer concentration (C_1), the total volumetric number density of clusters (N_v), and the average cluster radius ($\bar{r}$). For the later two quantities, only clusters of size greater than a threshold value (e.g., $n > 10$ in our example) are counted. This threshold cluster size is an input parameter. The two quantities are calculated using the following equations:

$$N_v = C_n / V_{at}, \tag{12}$$

$$\bar{r} = \frac{\sum_{n=11}^{n_{max}} (r_n \cdot C_n)}{\sum_{n=11}^{n_{max}} C_n}. \tag{13}$$

Note that this class requires all variables ($C_1 - C_n$) as input. We use a MOOSE function *addRequiredCoupledVarWithAutoBuild* to automatically create these variable names as input. However, currently only variables C_n with n from 0 to ($n_{max} - 1$) can be created by this MOOSE function. Since C_0 does not exist, a dummy *AuxVariable* needs to be created in the input file. Accordingly, the results from Equations 12 and 13 do not include the cluster size of n_{max}. If n_{max} is sufficiently large, C_n is small so the results should not be affected. Nevertheless, we will find a solution to solve this minor problem in the future.

CiRateTheory and **CvRateTheory** classes. These two classes were previously implemented in Grizzly. In this work, we use them separately from the cluster dynamics model to solve Equations 10 and 11 to obtain the interstitial (C_i) and vacancy (C_v) concentration under irradiation. The steady-state vacancy concentration is used to calculate the radiation-enhanced factor for Cu diffusion, f_{irr}. This enhanced factor is used as an input parameter for the cluster dynamics model. Note that the two classes could be directly coupled to the cluster dynamics model. If direct coupling is used, the results in the early nucleation and growth stage will change but those in the late coarsening stage (the stage with which we are most concerned) will not be affected. In other words, the direct coupling would not change the results at long times but make the cluster dynamics model less flexible because many other defect evolution model also can be used to calculate f_{irr}. Therefore, the current approach has more flexibility but less complexity than the direct coupling approach.

Input file syntax. A test input file is created in the *"tests/cluster_dynamics_cu_precp"* directory. The blocks related to the cluster dynamics model are shown below. Comments are added so that users can conveniently modify the input file for other applications.

```
[GlobalParams]
  N = 50                    # Number of Cu clusters
  var_name_base = C_Cu_
  parameters = UO_Parameters
[]

[AuxVariables]
  [./C_Cu_0]                # This is a dummy variable for the postprocessor coupled variable
    family = SCALAR         # This should be declared because the default may not be SCALAR
    order = FIRST           # This should be declared because the default may not be FIRST
    initial_condition = 0.0
  [../]
[]

[CDCuPrecipitation]
  # N = 50                  # Number of Cu clusters, already been declared in the GlobalParams
  C0_Cu = 0.0134            # Initial Cu concentration in matrix, atomic fraction
  T = 563.15                # temperature, K
  a0 = 2.867E-10            # lattice constant, in unit of m
  Em_Cu = 2.29              # Cu atom diffusion activation energy, eV
  D0_Cu = 6.3E-5            # Cu atom diffusion prefactor, m^2/s
  Omega_k_Cu = 6255.0       # kB*K
  S_k_Cu = 0.866            # kB
```

```
  E0_Interface_Cu = 0.37   # Cu-Fe interface energy, J/m^2
  Rad_Enhance_Diff_f = 2.5E7 # Radiation-enhanced Cu diffusion factor
[]

[Postprocessors]
  [./nit]
    type = NumNonlinearIterations
  [../]

  [./C1]
    type = CDCuClusterAverage
    n_criti = 10   # Only n>10 clusters are used for calculating the average
                   # cluster radius and number density
    output_type = C1
  [../]

  [./ave_r]
    type = CDCuClusterAverage
    n_criti = 10   # Only n>10 clusters are used for calculating the average
                   # cluster radius and number density
    output_type = Ave_r
  [../]

  [./total_cluster_dens]
    type = CDCuClusterAverage
    n_criti = 10   # Only n>10 clusters are used for calculating the average
                   # cluster radius and number density
    output_type = Total_Cluster_Density
  [../]
[]
```

3.3 Code verification using two case studies

Two case studies are used to verify the correct implementation of the model, which has been merged into INL's Grizzly repository. Case I is a previously published model of Cu precipitation under electron irradiation in a Fe-1.34at.%Cu at 290 °C [13]. Case II is our recently calibrated model of Cu precipitation under neutron irradiation in a Fe-0.3at.%Cu at 300 °C [11], which is closer to the realistic RPV materials and irradiation conditions than the first case. In both cases the parameters are calibrated with small angle neutron scattering experiments for the same alloys under the same irradiation conditions. The parameters of the two cases are summarized in Table 1. Note the parameters listed above the shaded row in Table 1 are used as input parameters for the cluster dynamics model in Grizzly. The parameters listed below the shaded row are used as inputs for the rate theory calculations of interstitial and vacancy evolution in Grizzly. The resulting radiation-enhanced Cu diffusion factors are listed immediately above the shaded row. In both case studies, the maximum cluster size is set to 1000 for demonstration purposes. To verify the correct implementation of the model in Grizzly, independent simulations using our standalone code, which is solved by the SUNDIALS ODE solver [14], are conducted for the same parameter sets of the two case studies.

First the time evolution of interstitial and vacancy concentration under irradiation is calculated using the

Parameter	Case I	Case II
Irradiation Type	Electron irradiation	Neutron irradiation
C_1^0, initial Cu concentration	1.34 at.%	0.3 at.%
a_0, lattice constant of bcc Fe	2.867 Å	same
T, temperature	563 K (290℃)	573 K (300 ℃)
E_{Cu}^m, activation energy of Cu thermal diffusion in Fe	2.29 eV	same
D_{Cu}^0, prefactor of Cu thermal diffusion in Fe	6.3×10^{-5} m^2/s	same
Ω, heat of mixing of Cu in Fe	6255 $k_B \cdot K$	same
ΔS, non-configurational entropy	$0.866 \cdot k_B$	same
σ, interface energy for coherent Cu-Fe interface	0.37 (J/m^2)	same
f_{irr}, Radiation enhanced factor	2.5×10^7	7.69×10^5
G_0, defect production rate	2×10^{-9} dpa/s	1.4×10^{-7} dpa/s
ε, cascade efficiency	1.0	0.4
ρ_d, dislocation density	1.0×10^{12} m^{-2}	5×10^{13} m^{-2}
E_i^m, Fe interstitial migration energy	0.3 eV	same
D_i^0, Fe interstitial diffusion prefactor	4.0×10^{-8} m^2/s	same
E_v^m, Fe vacancy migration energy	1.3 eV	1.0 eV
D_v^0, Fe vacancy diffusion prefactor	1.0×10^{-4} m^2/s	same
r_{iv}, defect recombination radius	6.5 Å	same
z_i, dislocation absorption efficiency for interstitials	1.2	same
z_v, dislocation absorption efficiency for vacancies	1.0	same
E_v^f, vacancy formation energy in Fe	1.6 eV	same

Table 1: Parameters of two cases studies. The Case I study is for Cu precipitation in a Fe-1.34at.%Cu at 290 °C under electron irradiation [13] and Case II is for Cu precipitation in a Fe-0.3at.%Cu at 300 °C under neutron irradiation [11] .

previously implemented *CiRateTheory* and *CvRateTheory* classes in Grizzly for the two case studies. The results are shown in Fig. 2. The steady state is reached at about 104 seconds in Case I while it is about 1 second in Case II. In both cases, the vacancy concentration is higher than the interstitial concentration at the steady state because dislocations absorb more interstitials than vacancies (the so called "dislocation bias"). At the steady state, the radiation enhanced Cu diffusion factor, $f_{irr} = C_v^{irr}/C_v^{th}$, is 2.5×10^7 in Case I and 7.69×10^5 in Case II. The enhanced factor is used as an input parameter for the cluster dynamics model in each case study, as shown in Table 1.

Next the Case I study of Cu precipitation is conducted in Grizzly. In this model, the alloy is Fe-1.34at.%Cu and the dislocation density is $\rho_d = 10^{12} m^{-2}$. The irradiation conditions are electron irradiation at 290 °C with a dose rate of 2×10^{-9} dpa/s. The parameters have been calibrated using the cluster number density and average cluster radius measured from small-angle neutron scattering experiments. Since electron irradiation only produces Frenkel pairs, the cascade efficiency is $\epsilon = 1.0$. The time (or dose) evolution of total Cu cluster number density and average radius is shown in Fig. 3. Here only clusters having more than 10 Cu atoms are counted. Clearly, Grizzly produces results that are nearly identical to those from the standalone code, indicating that the code implementation in Grizzly works correctly. The small difference between two codes may be induced by different solvers and converge criteria. At long times, both cluster number density and average radius reach saturated values. This behavior occurs simply because the maximum cluster size used in this demonstration case is not large enough.

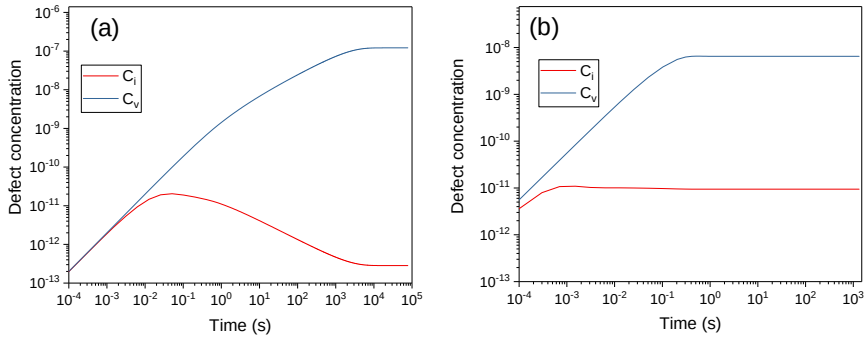

Figure 2: Time evolution of the interstitial and vacancy concentration under irradiation for two case studies. The steady-state vacancy concentration is used to calculate the radiation-enhanced Cu diffusion factor in each study. (a) Case I: Electron irradiation in a Fe-1.34at.%Cu at 290 °C. (b) Case II: Neutron irradiation in a Fe-0.3at.%Cu at 300 °C.

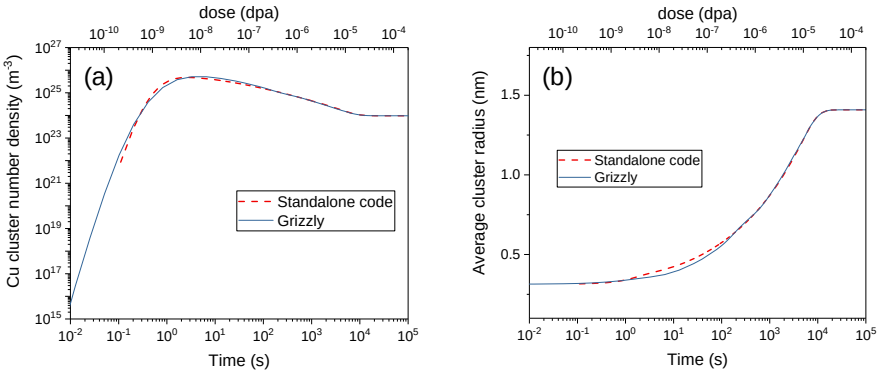

Figure 3: Time (bottom axis) and dose (top axis) evolution of Cu precipitation kinetics in a Fe-1.34at.%Cu at 290 °C under electron irradiation (Case I). (a) Evolution of total Cu cluster number density. (b) Evolution of average Cu cluster radius.

Similar to Case I, a study of Case II was also conducted using Grizzly. In this case, the alloy is a Fe-0.3at.%Cu alloy, the irradiation temperature is 300 °C, the dose rate is 1.4×10^{-7} dpa/s, and the dislocation density is $\rho_d = 5 \times 10^{13} m^{-2}$. Since both material properties and irradiation conditions are different from Case I, the parameters need re-calibration. Our recent work [11] shows that most of the parameters from Case I can be applied for Case II, except for the cascade efficiency and vacancy migration energy. Since neutron irradiation produces dense cascades and many defects recombine directly within the cascades, the cascade efficiency is set to $\epsilon = 0.4$. When Cu concentration is lower, the solute drag effect on the vacancy diffusion is also weaker. So the vacancy migration energy is changed to 1.0 eV to account for this effect. Similar to Case I, the new parameter set has been validated using the experimental data from small-angle neutron scattering experiments. The time (or dose) evolution of total Cu cluster number density and average radius for the Fe-0.3at.%Cu alloy is shown in Fig. 4. Again here only clusters having more than 10 Cu atoms are counted. Again, Grizzly produces nearly identical results as the standalone code does. The discrepancy is a little larger than that in Case I. But overall the agreement is excellent.

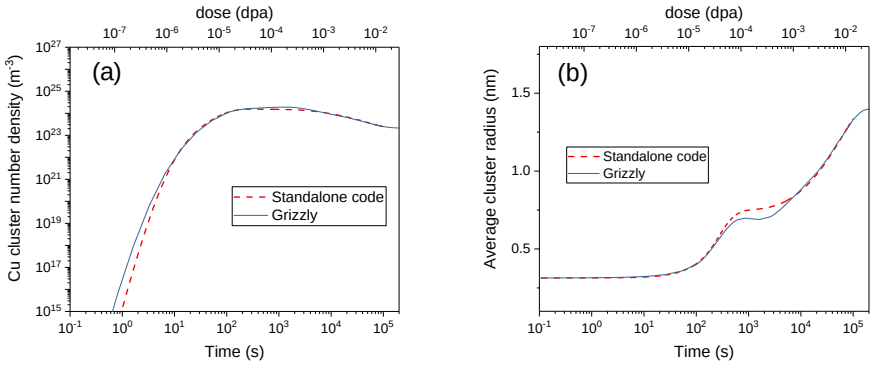

Figure 4: Time (bottom axis) and dose (top axis) evolution of Cu precipitation kinetics in a Fe-0.3at.%Cu at 300 °C under neutron irradiation (Case II). (a) Evolution of total Cu cluster number density. (b) Evolution of average Cu cluster radius.

3.4 Discussions and conclusions

In FY17, we have successfully implemented the cluster dynamics model of Cu precipitation under irradiation in MOOSE based Grizzly. This implementation will enable a direct coupling of the cluster dynamics model with other MOOSE-based applications directly. The code takes advantages of many built-in MOOSE features. It has an architecture which will enable convenient modification or expansion of the code capability in the future. The input file was made as simple as possible so that non-experts can easily use the code. The cluster dynamics model can be coupled to plasticity models in Grizzly. It can also be extended to model the precipitation of Mn-Ni-Si clusters in the future. Currently the efficiency of the code is not as good as our standalone code, possibly due to some problems of the ODE solvers in the PETSc package (which is mainly used for solving partial differential equations (PDEs)). We will work with the MOOSE team to find a solution. An alternative solution is to implement the grouping method [15] to improve the efficiency of the code.

4 Cu precipitate induced embrittlement in crystal plasticity

Irradiation-induced defects, including copper rich precipitates (CRP) and self-interstitial atom (SIA) loops, contribute to the long-term failure risks of RPV steels through embrittlement of the steel [1, 10]. These irradiation defects act as obstacles to dislocation motion, and the impeded dislocation motion at the microstructure scale produces an increase in the yield stress and significant hardening in the plastic regime of the material behavior on an engineering scale. Crystal plasticity models, which predict dislocation density evolution in an irradiation damaged microscale structure, can be used to connect microstructure evolution to macroscale behavior predictions.

In previous years, a monolithic code crystal plasticity model was developed to predict the yield stress increase and plastic hardening behavior of BCC-iron with different static quantities of irradiation defects (CPR and SIA loops) from experimental data [7, 16, 17]. In FY16, this existing model was validated against experimental data [18] and was coupled with a microplane damage model to capture anisotropic cleavage fracture [7]. The significant changes of the RPV steel microstructure evolution, as described in previous sections of this report, affect the crystal plasticity simulations which use the microstructure state as initial conditions for the model internal state variables. The coupling of the crystal plasticity model to the microscale models is a critical component of predicting macroscale property changes in response to microscale evolution, eliminating the need for static initial conditions of the irradiation defects. Under the Grizzly project in FY17 an effort was made to couple the crystal plasticity model to results from microscale dislocation dynamics and cluster dynamics models. This effort included implementing a new dislocation cross slip model to capture stochastic dislocation interactions from dislocation dynamics models and incorporating cluster dynamics results for CRP characteristics directly into the crystal plasticity model.

4.1 Model description and implementation

Dislocation density based crystal plasticity models calculate the stress and plastic strain resulting from dislocation motion, evolution, and interaction with microstructure features including other dislocations and irradiation defects. Dislocation motion, the motion of plastic slip, on each individual slip system is summed to calculate the plastic velocity gradient:

$$L^P = \sum_{\alpha} \dot{\gamma}^{(\alpha)} \hat{s} \otimes \hat{m}, \quad \text{where} \quad \dot{\gamma}^{\alpha} = \rho^{(\alpha)}_{mobile} b v_{glide} \tag{14}$$

In the dislocation density based crystal plasticity mode, the Orowan relation is used to calculate the dislocation glide slip as a function of the mobile dislocation density, burgers vector, and dislocation glide velocity [19]. In a continuum crystal plasticity model, the dislocation glide velocity is modeled as a function of the applied shear stress on the slip system and the slip system resistances; within this crystal plasticity model we apply an enthalpy driven flow rule [20]. The evolution of dislocations is separated into two categories, mobile dislocations:

$$\dot{\rho}^{(\alpha)}_{mobile} = \frac{k_{mult}}{b} \sqrt{\sum_{\beta} \rho^{(\beta)}_{mobile}} |\dot{\gamma}^{(\alpha)}| - \frac{2R_c}{b} \rho^{(\alpha)}_{mobile} |\dot{\gamma}^{(\alpha)}| - \frac{1}{b\beta_p \sqrt{\rho^{(\alpha)}_{mobile} + \rho^{(\alpha)}_{immobile}}} |\dot{\gamma}^{(\alpha)}| \tag{15}$$

and immobile dislocations:

$$\dot{\rho}^{(\alpha)}_{immobile} = \frac{1}{b\beta_p \sqrt{\rho^{(\alpha)}_{mobile} + \rho^{(\alpha)}_{immobile}}} |\dot{\gamma}^{(\alpha)}| - k_{dyn} \rho^{(\alpha)}_{immobile} |\dot{\gamma}^{(\alpha)}| \tag{16}$$

In Equations 15 and 16, k_{mult} is the coefficient for the multiplication of dislocations with the Frank-Reed generation mechanism, R_c is the radius of interaction between two dislocations with opposite signs on the

same slip plane, k_{dyn} is the coefficient for the dynamic recovery of immobile dislocations, and β_d is the coefficient for the contribution of the total dislocation forest to the mean free glide path for mobile dislocations. Note the coupling among the trapped mobile dislocations, the third term in Equation 15, and the generation of immobile dislocations, the source term in Equation 16.

The resistance to dislocation glide velocity is divided into athermal and thermal resistance to slip in the enthalpy flow rule. Thermal resistance is an intrinsic material property from the lattice friction, and athermal resistance is a function of the microstructure of the grain. Here we have defined the athermal resistance as a function of dislocations and CRP particles:

$$s^{(\alpha)}_{athermal} = q_d G b \sqrt{\sum_{\beta} A^{\alpha\beta} \left(\rho^{(\beta)}_{mobile} + \rho^{(\beta)}_{immobile} \right)} + q_c G b \lg \left(\frac{1}{2b\sqrt{N \times d}} \right) \sqrt{N \times d} \tag{17}$$

where resistance due to dislocations is modeled with a Bailey-Hirsch type expression and resistance due to copper clusters is modeled in the vein of Kotrecho [18]. In Equation 17 q_d is the coefficient for total dislocation barrier resistance to mobile dislocation glide, q_c is the coefficient for the Kotrecho barrier hardening model for CRPs, G is the shear modulus, N is the number density of CRP irradiation defects, and d is the mean diameter of the CRP irradiation defects.

Material Model Implementation. A significant portion of the FY17 crystal plasticity effort centered on updating the Grizzly crystal plasticity model to the current MOOSE `tensor_mechanics` module plug-and-play system. The code updating effort is necessary to both maintain the code as the MOOSE framework changes and to set the ground work for coupling to microstructure models, including cluster dynamics, through the MOOSE framework. The `tensor_mechanics` plug-and-play system separates the calculation of stress, strain, and the elasticity tensor into different classes. This separation enables more flexibility in simulations while reducing code duplication.

The code updating effort in FY17 recast as a `StressUpdateBase` type material. `StressUpdateBase` materials are atypical materials in that MOOSE/Grizzly do not directly call these materials so that these materials can iterate to solve for internal state variables, e.g. slip increments and mobile dislocation density increments. A base class for general crystal plasticity, `CrystalPlasticityUpdate` was written to allow the inheriting crystal plasticity classes to focus solely on implementing slip and dislocation evolution constitutive equations while the base class handles the iteration schemes. The use of the base class significantly reduces the amount of code duplication in the Grizzly crystal plasticity models. The dislocation density based model described here is implemented as `CrystalPlasticityEnthalpyFlowRuleUpdate` and is undergoing preparation to be merged into Grizzly.

Simulation Parameters. The parameters for the `StressUpdate` crystal plasticity model were calibrated with the unirradiated Fe-0.3%Cu experimental data from [16], based in part on the calibration of the FY16 monolithic crystal plasticity model [7]. The parameter calibration simulations were performed on a single 1x1x1 mm^3 cubic grain loaded in the [1 0 0] direction (along the x-axis). In all of the crystal plasticity simulations discussed in this report, an initial mobile dislocation density of 40 m^{-2} and an immobile dislocation density of 50 m^{-2}, corresponding to the experimental data of [16], were used.

These parameters in Table 2 are similar to the values calibrated for α-iron [18], excepting the parameter for dislocation multiplication. The re-calibration of this parameter for the Fe-0.3%Cu system is supported by the discussion in [21]: solute atoms in alloys can promote higher dislocation multiplication [18].

4.2 Cross slip formulation comparison

In lower length scale models, such as dislocation dynamics, the probability of cross slip is calculated as a stochastic process [22] for single dislocations. At the continuum level in crystal plasticity models, the

Crystal Plasticity Parameter	Parameter Value
Dislocation multiplication coefficient (k_{mult})	0.32
Dynamic immobilization recovery coefficient (k_{dyn})	100
Radius of dislocation interaction (R_c)	8 nm
Dislocation forest hardening coefficient (β_d)	0.4
Dislocation barrier hardening resistance (q_d)	0.2
CRP irradiation defect barrier hardening (q_c)	0.02

Table 2: Crystal plasticity model parameters calibrated for Fe-0.3%Cu with experimental data [16]

challenge is how to handle cross slip calculations with dislocation densities instead of single dislocations.

In the deterministic cross slip approach [20] originally implemented in the Grizzly crystal plasticity model [7], the model simply determines which slip system has the highest probability of receiving cross slip dislocations within the cross slip family. This single slip system then receives all of the cross slip dislocations from all other slip systems within the cross slip family at every simulation time step.

In FY17 we added a new stochastic approach for calculating cross slip in the crystal plasticity model because cross slip is a significant component of dislocation motion in BCC materials [23]. The stochastic approach calculates the probability of cross slip for each slip system within a single cross slip family using the same probability function from dislocation dynamics [22, 24]. We construct a continuous distribution function (CDF) for the cross slip family from normalized individual slip system probabilities. The CDF has a step function appearance, consisting of normalized probability bins for the likelihood that a certain system will receive cross slip dislocations, and the slip system with the highest applied stress have largest probability bin in the CDF vector. The total CDF is bounded from 0 to 1. We then perform a Monte Carlo type analysis to determine which slip systems receive cross slip dislocations from the other slip systems within the family.

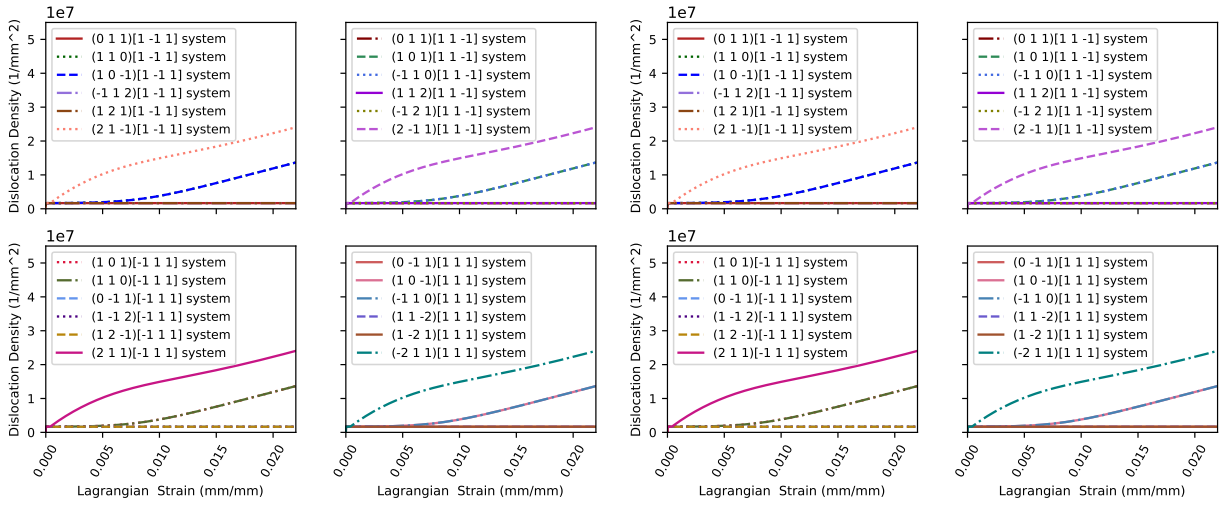

Figure 5: Comparison of the cross slip models in a single grain loaded along the [1 0 0] direction. The left figure shows the deterministic cross slip model results, separated by cross slip family, with mobile dislocation densities; the right figure shows the results from the stochastic cross slip model, also separated by cross slip family, with the mobile dislocation densities per slip system. Under this loading direction both cross slip models demonstrate similar impacts on the active mobile dislocation evolution, as expected under loading conditions with multiple slip systems activated.

The comparison simulations of the cross slip models were performed using only 24 slip systems, a reasonable assumption at lower temperatures [24], to simplify the cross slip comparison figures. We ran two sets of cases to compare the cross slip models in different loading conditions: in the [1 0 0] direction (along the x-axis) and in the [-3 4 8] direction. The [1 0 0] loading direction actives four slip systems equally, Figure 5, one in each cross slip family, while the [-3 4 8] loading direction, Figure 6, is selected to activate only a single slip system.

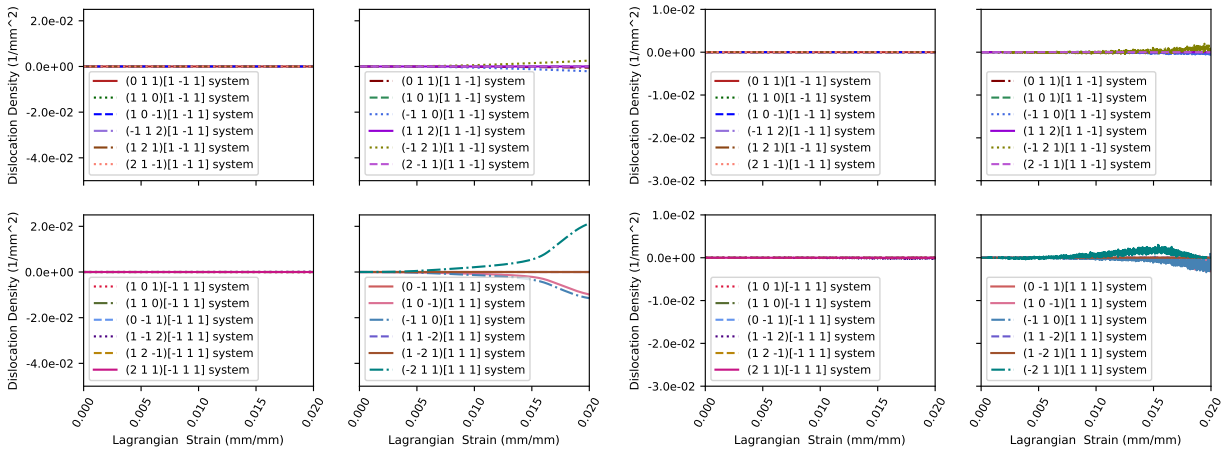

Figure 6: Comparison of the deterministic (left figure) and the stochastic (right figure) cross slip models in a single grain loaded in the [-3 4 8] direction with cross slipped dislocation densities shown. This loading direction is expected to activate only a single slip system. The deterministic cross slip model (left) demonstrates limitations in this loading direction by locking the cross slip dislocation contributions to a single slip system while the stochastic cross slip model (right) allows the cross slip dislocation contributions to continue to evolve and therefore avoids over-hardening the crystal stress response.

The stochastic cross slip approach enables the crystal plasticity model to capture single slip system activation under specific loading conditions while the deterministic approach locks the contributions of the cross slipped dislocations to specific slip systems, see Figure 6. This ability to activate a single slip system is key to the correct fitting of material parameters within the crystal plasticity model from lower length scale models, such as dislocation dynamics, or precise experimental data when only a single slip system is activated in the test.

4.3 Coupling to cluster dynamics CRP results

We completed the coupling of crystal plasticity to cluster dynamics results in FY17 through the implementation of functions to calculate the characteristics of the CRP defects: cluster density (N) and mean precipitate diameter (d). These functions were calculated by fitting the FY16 cluster dynamics model results [7]

$$ln(N)(m^{-3}) = 52.398 - 0.0049 \cdot ln(dpa)^4 - 0.0931 \cdot ln(dpa)^3 - 0.6037 \cdot ln(dpa)^2 - 2.1621 \cdot ln(dpa) \quad (18)$$

$$d(nm) = 4.1926 \cdot dpa^{0.2558} \quad (19)$$

We note that Equations 18 and 19 calculate a larger cluster density and a slightly smaller cluster radius than those experimental values reported by [16]. The simulation results presented below include only irradiation effects from the CRP defects; the contribution to irradiation embrittlement from SIA loops is not included in these results to isolate the impact of the CRP defects on the crystal plasticity simulation results.

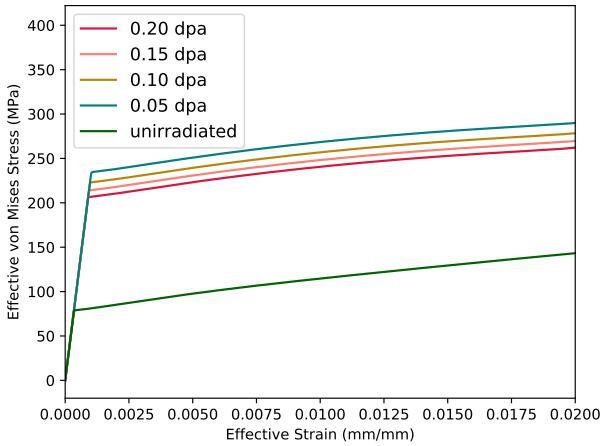

Figure 7: Response of the coupled crystal plasticity and cluster dynamics results to neutron irradiation doses, where only CRPs are considered as irradiation defects, in a single grain loaded in the [1 0 0] direction. The presence of the CRPs result in an increased yield stress response.

The single grain results demonstrate the expected increase in the yield strength under added irradiation dose. We note that the downward trend in yield stress with increasing irradiation dose is expected in the 0.5dpa to 2.0 dpa neutron irradiation dose range modeled here: the CRP cluster density decreases by almost an order of magnitude in the range of 0.01 dpa to 1.0 dpa in the cluster dynamics results [7]. The results in Figure 7 demonstrate a lower yield stress for the neutron irradiation dose than reported in experimental data [16, 17] because these simulations excluded the hardening effects of SIA loop and included only the embrittlement effects of the CRP defects. Nonetheless, these results demonstrate the coupling crystal plasticity to cluster dynamics with the results of the cluster dynamics simulations to calculate the characteristics of the CRP irradiation defects.

4.4 Discussion and conclusions

Our efforts in FY17 have focused on establishing the ground work to enable coupling between crystal plasticity and microstructure models, particularly cluster dynamics. The coupled crystal plasticity-cluster dynamics model enables the on-demand calculation of CRP characteristics for a specified neutron irradiation dose. The implementation of the existing Grizzly crystal plasticity model into the current MOOSE `tensor_mechanics` plug-and-play framework will ease the future process of coupling these models. We have also implemented an additional method of calculating cross slip to allow for the activation of a single slip system within the crystal plasticity simulations under specific loading conditions. This new ability to replicate the activation of a single slip system will enable better model parameter fitting against microstructure models such as dislocation dynamics. We will continue to verify and validate the crystal plasticity model as coupling to cluster dynamics simulations continues.

5 Summary

In FY17, progress has been made in coupling lower-length-scale models developed to predict microstructure evolution and the resulting macroscopic property degradation in reactor pressure vessel steels. In FY17 a cluster dynamics model was implemented in Grizzly for radiation damage, and an effort was couple the cluster dynamics model to lattice kinetic Monte Carlo model to capture irradiation enhanced diffusion effects in precipitate formation. For hardening and embrittlement, effort was made to couple the dislocation-density based crystal plasticity model to cluster dynamics simulation results..

These accomplishments have increased the Grizzly capability for modeling microstructure evolution and property degradation, and also made broad impact in the research community. The research and development outcome has led to the publication of one journal publication and four presentations at leading conferences, as detailed below.

Journal publications:

1. X. Bai, H. Ke, Y. Zhang, and B. W. Spencer, Modeling Copper Precipitation Hardening and Embrittlement in A Dilute Fe-0.3at.%Cu Alloy Under Neutron Irradiation, Journal of Nuclear Materials, Accepted, 2017

Conference presentations:

1. X.M. Bai, Multiscale modeling of radiation hardening in reactor pressure vessel steels, 2017 International Conference on Plasticity, Damage, and Fracture, Puerto Vallarta, Mexico, Jan 2017, **Invited talk**.

2. X.M. Bai, H. Ke, P. Chakraborty, Y. Zhang, Cluster Dynamics Modeling of Cu Precipitation Hardening in Reactor Pressure Vessel Steels, 2017 TMS Annual Meeting, San Diego, CA, Feb-Mar 2017.

3. S.A. Pitts, W. Jiang, B.W. Spencer, H.M. Zbib, Comparison of Irradiated Steel Dislocation and Defect Interaction Models with Crystal Plasticity, Engineering Mechanics Institute Conference 2017, San Diego CA, June 2017

4. Y. Zhang, X. Bai, M. Tonks, B. Biner, Formation of prismatic loops from C15 phase interstitial clusters in body-centered-cubic iron, Society of Engineering Science Meeting 2017, Boston MA, July 2017

6 References

[1] G. Odette and G. Lucas. "Embrittlement of Nuclear Reactor Pressure Vessels". In: *Journal of Materials* 57 (2001), pp. 18–22.

[2] K. Farrell, T. S. Byun, and N. Hashimoto. "Deformation mode maps for tensile deformation of neutron-irradiated structural alloys". In: *Journal of Nuclear Materials* 335 (2004), p. 471.

[3] E. Meslin, M. Lambrecht, M. Hernandez-Mayoral, F. Bergner, L. Malerba, P. Pariege, B. Radiguet, A. Barbu, D. Gomez-Briceno, A. Ulbricht, and A. Almazouzi. "Characterization of neutron-irradiated ferritic model alloys and a RPV steel from combined APT, SANS, TEM and PAS analyses". In: *Journal of Nuclear Materials* 406 (2010), pp. 73–83.

[4] D. J. Bacon, Y. N. Osetsky, and D. Rodney. "Dislocation-Obstacle Interactions at the Atomic Level". In: Elsevier, 2009. Chap. 88.

[5] B. Spencer, Y. Zhang, P. Chakraborty, S. B. Biner, M. Backman, B. Wirth, S. Novascone, and J. Hales. *Grizzly Year-End Progress Report*. Tech. rep. INL/EXT-13-30316. Idaho National Laboratory, Sept. 2013.

[6] Y. Zhang, D. Schwen, H. Ke, X. Bai, and J. Hales. *Mesoscale modeling of solute precipitation and radiation damage*. Tech. rep. Idaho National Laboratory, Sept. 2015.

[7] Y. Zhang, P. Chakraborty, X. Bai, and D. Schwen. *Lower Length Scale Model Development for Embrittlement of Reactor Pressure Vessel Steel*. Tech. rep. Idaho National Laboratory, Sept. 2016.

[8] B. Spencer, Y. Zhang, P. chakraborty, M. Backman, W. Hoffman, D. Schwen, S. B. Biner, and X. Bai. *Grizzly status report*. Tech. rep. Idaho National Laboratory, Sept. 2014.

[9] P. Chakraborty, S. B. Biner, Y. Zhang, and B. Spencer. *Crystal Plasticity Model of Reactor Pressure Vessel Embrittlement in Grizzly*. Tech. rep. Idaho National Laboratory, July 2015.

[10] C. English and J. Hyde. "Radiation Damage of Reactor Pressure Vessel Steels". In: *Comprehensive Nucl. Mater.* 4 (2012), pp. 151–180.

[11] X. Bai, H. Ke, Y. Zhang, and B. W. Spencer. "Modeling Copper Precipitation Hardening and Embrittlement in A Dilute Fe-0.3at.%Cu Alloy Under Neutron Irradiation". In: *Accepted by the Journal of Nuclear Materials* (2017).

[12] Y. Zhang, P. C. Millett, M. R. Tonks, X.-M. Bai, and S. B. Biner. "Preferential Cu precipitation at extended defects in bcc Fe: An atomistic study". In: *Computational Materials Science* 101 (2015), pp. 181–188.

[13] F. Christien and A. Barbu. "Modelling of copper precipitation in iron during thermal aging and irradiation". In: *Journal of Nuclear Materials* 324 (2004), p. 90.

[14] *SUNDIALS: SUite of Nonlinear and DIfferential/ALgebraic Equation Solvers*. 2017.

[15] S. I. Golubov, A. M. Ovcharenko, A. V. Barashev, and B. N. Singh. "Grouping method for the approximate solution of a kinetic equation describing the evolution of point-defect clusters". In: *Philosophical Magazine A* 81.3 (2001), pp. 643–658.

[16] M. Lambrecht, L. Malerba, and A. Almazouzi. "Influence of different checmical elements on irradiation-induced hardening embrittlement of RPV steels". In: *Journal of Nuclear Materials* 378 (2008), pp. 282–290.

[17] M. Lambrecht, E. Meslin, L. Malerba, M. Hernandez-Mayoral, F. Bergner, P. Pariege, B. Radiguet, and A. Almazouzi. "On the correlation between irradiation-induced microstructural features and the hardening of reactor pressure vessel steels". In: *Journal of Nuclear Materials* 406 (2010), pp. 84–89.

[18] P. Chakraborty and S. B. Biner. “Crystal plasticity modeling of irradiation effects on flow stress in pure-iron and iron-copper alloys”. In: *Mechanics of Materials* 101 (2016), pp. 71–80.

[19] E. Orowan. “Problems of plastic gliding”. In: *Proceedings of the Physical Society* 52.1 (1940), p. 8.

[20] A. Patra and D. L. McDowell. “Continuum modeling of localized deformation in irradiated bcc materials”. In: *Journal of Nuclear Materials* 432.1 (2013), pp. 414–427.

[21] C. Schmidt and A. Miller. “The effect of solutes on the strength and strain hardening behavior of alloys”. In: *Acta Metallurgica* 30.3 (1982), pp. 615–625.

[22] H. M. Zbib, M. Rhee, and J. P. Hirth. “On plastic deformation and the dynamics of 3D dislocations”. In: *International Journal of Mechanical Sciences* 40.2-3 (1998), pp. 113–127.

[23] W. Püschl. “Models for dislocation cross-slip in close-packed crystal structures: a critical review”. In: *Progress in materials science* 47.4 (2002), pp. 415–461.

[24] D. Li, H. Zbib, X. Sun, and M. Khaleel. “Predicting plastic flow and irradiation hardening of iron single crystal with mechanism-based continuum dislocation dynamics”. In: *International Journal of Plasticity* 52 (2014), pp. 3–17.